Cell, Vol. 86, 209–219, July 26, 1996, Copyright ©1996 by Cell Press

Myelination in the Absence of Galactocerebroside and Sulfatide: Normal Structure with Abnormal Function and Regional Instability

Timothy Coetzee,[1,7] Nobuya Fujita,[1,7] Jeffrey Dupree,[1] Riyi Shi,[3] Andrew Blight,[3] Kinuko Suzuki,[1,2] Kunihiko Suzuki,[1,4,6] and Brian Popko,[1,5,6]
[1] UNC Neuroscience Center
[2] Department of Pathology and Laboratory Medicine
[3] Department of Surgery
Division of Neurosurgery
[4] Department of Neurology and Psychiatry
[5] Department of Biochemistry and Biophysics
[6] Program in Molecular Biology and Biotechnology
University of North Carolina at Chapel Hill
Chapel Hill, North Carolina 27599

Summary

The vertebrate nervous system is characterized by ensheathment of axons with myelin, a multilamellar membrane greatly enriched in the galactolipid galactocerebroside (GalC) and its sulfated derivative sulfatide. We have generated mice lacking the enzyme UDP-galactose:ceramide galactosyltransferase (CGT), which is required for GalC synthesis. CGT-deficient mice do not synthesize GalC or sulfatide but surprisingly form myelin containing glucocerebroside, a lipid not previously identified in myelin. Microscopic and morphometric analyses revealed myelin of normal ultrastructural appearance, except for slightly thinner sheaths in the ventral region of the spinal cord. Nevertheless, these mice exhibit severe generalized tremoring and mild ataxia, and electrophysiological analysis showed conduction deficits consistent with reduced insulative capacity of the myelin sheath. Moreover, with age, CGT-deficient mice develop progressive hindlimb paralysis and extensive vacuolation of the ventral region of the spinal cord. These results indicate that GalC and sulfatide play important roles in myelin function and stability.

Introduction

The myelin sheath is a multilamellar, spirally wrapping extension of the plasma membranes of oligodendrocytes in the central nervous system (CNS) and of Schwann cells in the peripheral nervous system (PNS) (reviewed in Morell et al., 1994). This specialized structure exhibits a low capacitance and as a result serves as an axonal insulator that facilitates transmission of nerve impulses by saltatory conduction. The end result is a reduction in the energy and space utilization requirements of the nerve cell. Since several human disease states such as multiple sclerosis, Pelizeaus–Merzbacher disease, Charcot–Marie–Tooth disease, metachromatic leukodystrophy, and globoid leukodystrophy result from deficiency or disruption of myelin, understanding the nature of this specialized membrane is of practical importance.

Biochemically, myelin exhibits a unique composition with >70% of the dry weight consisting of lipids and the remainder being comprised of a relatively simple array of myelin-specific proteins (Morell et al., 1994). Significant insights into the structural and functional properties of the sheath have been gained from studies of naturally occurring and experimentally induced rat and mouse mutants defective in these proteins (Campagnoni and Macklin, 1988; Giese et al., 1992; Boison and Stoffel, 1994; Li et al., 1994; Montag et al., 1994; Adlkofer et al., 1995; Lunn et al., 1995). With the exception of mice lacking myelin-associated glycoprotein (MAG) (Li et al., 1994; Montag et al., 1994), analysis of these mutants has shown that elimination of the structural myelin proteins disrupts the myelination process and, as a consequence, disrupts the proper function of the nervous system. In the case of MAG, mice lacking this quantitatively minor myelin component form functional myelin that exhibits only subtle morphological abnormalities.

In contrast to the myelin proteins, relatively little is known about the functional importance of myelin lipids. Among the most abundant myelin lipids are galactocerebroside (GalC) and its sulfated derivative, sulfatide, which together constitute ~27% of the myelin lipid (Norton and Cammer, 1984). This abundance has led to the suggestion that GalC and sulfatide have an important role in the structure of myelin (Curalto, 1987). In addition, a number of studies have suggested that GalC may have a function in the development of oligodendrocytes. GalC is one of the earliest markers denoting differentiation of oligodendrocytes from the O2A precursor to an immature oligodendrocyte (Pfeiffer et al., 1993), and anti-GalC antibodies reversibly inhibit differentiation of immature oligodendrocytes into mature oligodendrocytes (Bansal and Pfeiffer, 1989). These observations suggest that GalC may be transducing signals essential to maturation of oligodendrocytes. This possibility is further supported by studies demonstrating that anti-GalC antibodies induce calcium flux across oligodendrocyte membranes and subsequent rearrangement of microtubules (Dyer and Benjamins, 1988, 1989, 1990, 1991). Additional studies have shown that anti-GalC antibodies inhibit myelination in vitro and in vivo (Fry et al., 1974; Dorfman et al., 1979; Ranscht et al., 1987; Rosenbluth et al., 1994). Together, these studies raise the intriguing possibility that GalC functions in processes essential to oligodendrocyte development and subsequent myelination (Benjamins and Dyer, 1990; Dyer, 1993).

GalC is synthesized by addition of galactose to ceramide in a single step with UDP-galactose as the donor (Morell and Radin, 1969). The enzyme responsible for this reaction is UDP-galactose:ceramide galactosyltransferase (CGT) (E. C. 2.4.2.62), a glycosylated microsomal enzyme consisting of 541 amino acids with a molecular weight of ~61 kDa (Morell and Radin, 1969; Neskovic et al., 1986; Schulte and Stoffel, 1993; Stahl et al., 1994; Schaeren-Wiemers et al., 1995). Previously, we and others reported the isolation and characterization of rat cDNA clones encoding CGT (Schulte and

[7] The first two authors contributed equally to this work and are listed alphabetically.

Stoffel, 1993; Stahl et al., 1994; Schaeren-Wiemers et al., 1995). These studies showed that CGT is abundantly expressed in the actively myelinating CNS and PNS, consistent with its role in myelination. Subsequently, we have isolated and characterized genomic clones containing the mouse *Cgt* gene, which is composed of six exons located on chromosome 3 (Coetzee et al., 1996).

Given the number of functions attributed to GalC, we have attempted to ascertain the effect of elimination of this lipid on the development and function of the nervous system. We have found that CGT-deficient mice cannot synthesize GalC or sulfatide and yet are able to form compact myelin. This report describes the consequences of the lack of CGT on the clinical, pathological, biochemical, and electrophysiological phenotype of these animals.

Results

Disruption of the Mouse *Cgt* Gene

The targeting vector (pPNTCGT) was generated by inserting the neomycin resistance gene (*neo*) into a KpnI site present within exon 2, 219 nt downstream of the initiation codon of the *Cgt* gene (Figure 1A) (Coetzee et al., 1996). NotI-linearized pPNTCGT was electroporated into BK4 ES cells, a subclone of line E14TG2a, and neomycin resistant clones selected using G418. Following selection, 52 ES clones were isolated of which 14 carried the targeted recombination event as determined using a probe outside the targeting construct (Probe A, Figure 1A; data not shown).

Targeted ES cells were injected into C57Bl/6J blastocysts and 16 chimeric animals generated. Five males and one female transmitted the targeted allele to germline cells. Heterozygote F1 animals were interbred to generate homozygote *Cgt*-deficient mice. The genotype was determined using an internal *Cgt*-specific probe (Probe B, Figure 1A). Probe B detected a 15 kb BamHI fragment in both wild type and heterozygotes but not homozygotes (Figure 1B). In addition, 8 and 9 kb fragments were detected in both heterozygotes and the homozygotes, but not in wild type (Figure 1B). These results are consistent with the predicted insertion of a unique BamHI site into the second exon of the targeted *Cgt* gene. Finally, Northern blot analysis of brain RNA indicated that expression of full-length *CGT* mRNA was abolished in the homozygote, and that a neomycin-containing truncated transcript was expressed in both heterozygote and homozygote animals (Figure 1C). Distribution of the −/− animals followed Mendelian segregation indicating that the −/− genotype was not embryonic lethal.

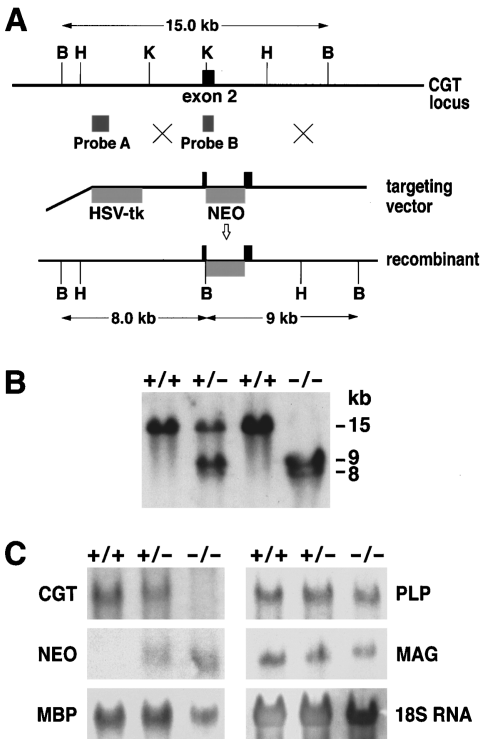

Figure 1. Targeted Disruption of the Mouse *Cgt* Locus

(A) A partial restriction map of the *Cgt* gene, targeting construct, and the expected replacement event are shown. The neomycin resistance gene (*neo*) was inserted into a KpnI (K) site located within exon 2, which contains the initiation codon and codes for the N-terminal half of the CGT enzyme. The relative locations of the screening probes (Probes A and B) are shown. The top double-headed arrow indicates the endogenous 15 kb BamHI fragment, detected by both probes, that is characteristic of the wild-type gene. The addition of the *neo* gene introduces a new BamHI site within the targeted allele. This site yields a diagnostic 8 kb BamHI fragment that is detected by both probes. Probe B also detects a 9 kb BamHI fragment corresponding to sequences downstream of the *neo* gene.

(B) Southern blot analysis of tail DNA from wild type (+/+), heterozygous (+/−), and homozygous (−/−) are shown. Tail DNA was digested with BamHI, and hybridized with probe B.

(C) Northern blot analysis of total RNA was isolated from brains of *Cgt* +/+, +/−, and −/− mice is shown. Total RNA separated by formaldehyde-agarose (0.8%) gel electrophoresis, transferred to nylon membranes, and probed for the expression of CGT, neomycin (NEO), myelin basic protein (MBP), proteolipid protein (PLP), and myelin-associated glycoprotein (MAG). All five RNA sets were run on the same gel in parallel and were loaded from master mixes of +/+, +/−, and −/− RNA. All five membranes were analyzed for 18S RNA and showed similar results.

Clinical Phenotype of *Cgt*$^{-/-}$ Mice

Heterozygotes have not exhibited a clinical phenotype throughout the first nine months of observation. No clinical phenotype was detectable in −/− mice until postnatal day (PND) 12–14, at which time *Cgt*$^{-/-}$ animals exhibited a gross jerking of the head and mildly ataxic locomotion. Between PND 16 and 20, tremoring became noticeable at rest and very pronounced during movement. Locomotion was characterized by splaying of the hindlimbs with clenching of the paws, dragging of the hindquarters, and vertical positioning of the tail. In addition, many animals clasped the hindlimbs to the body when held by the tail and showed a tendency to have closed eyes. No seizures were observed. Generally, −/− animals were smaller than littermates with body weight of one-half to two-thirds that of +/+ and +/− littermates. With age, −/− animals exhibited a progressive loss of function in the hindlimbs, such that by PND60 many animals had lost much of their ability to move, lay on their sides or back, and showed signs of labored breathing. Age at death of −/− mice was variable with

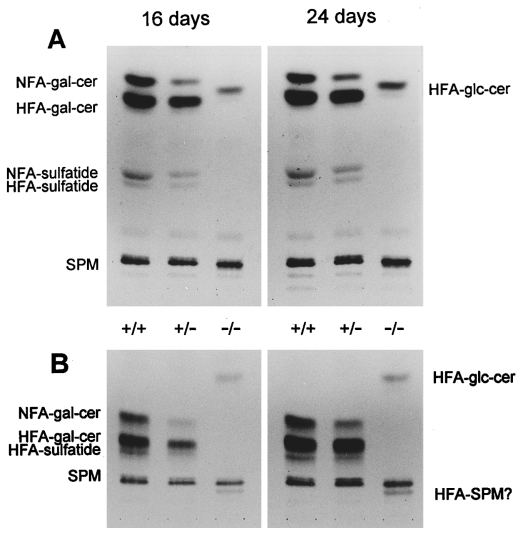

Figure 2. Analysis of Total Brain Lipids from *Cgt*$^{-/-}$ Mice

(A) Total brain lipids were extracted from brain of 16 and 24 day old *Cgt* +/+, +/−, and −/− mice, mercuric chloride-treated, saponified, and separated on HPTLC 60 plates at 3 mg–wet weight equivalent per sample. The solvent system was chloroform-methanol-water (70:30:4, v/v/v). Lipids were visualized with copper acetate spray and heating.

(B) Lipids were prepared as in (A) and separated by TLC on borate impregnated plates. The solvent system was chloroform-methanol-concentrated ammonia (70:30:5, v/v/v).

Abbreviations: NFA, normal fatty acid; HFA, α-hydroxy-fatty acid; glc-cer, glucocerebroside; SPM, sphingomyelin.

some animals dying around PND 18–30 and others surviving past PND 90. Female −/− animals are fertile but appear incapable of caring for their pups.

GalC Is Absent from Brain Lipids

Thin-layer chromatography (TLC) of the saponified total brain lipid fraction clearly showed that both normal fatty acid– (NFA-) and hydroxy-fatty acid– (HFA-) containing GalC and sulfatide were absent from the brain of the −/− mouse (Figure 2A). GalC and sulfatide levels were reduced in +/− animals compared with normal. In particular, the levels of NFA-GalC and NFA-sulfatide were reduced in 16-day-old +/− animals compared with +/+ control. No differences were seen in the levels of cholesterol, glycerophospholipids, and gangliosides (data not shown).

Interestingly, a conspicuous band displaying a mobility between NFA- and HFA-GalC was present only in the −/− fraction (Figure 2A). This mobility pattern was consistent with HFA-glucocerebroside (GlcC). The assignment of HFA-GlcC was supported by TLC on borate-impregnated plates. Under these conditions GalC exhibits a retarded mobility, whereas GlcC mobility is unaffected (Figure 2B). Additionally, a band was seen below the sphingomyelin band in the saponified −/− preparation on borate-impregnated plates (Figure 2B). The slower mobility suggested that this band corresponds to HFA-sphingomyelin. Visualization by both acid molybdate and anisaldehyde sprays gave blue colors expected for sphingomyelin.

Cgt$^{-/-}$ Mice Form Compact Myelin

Although Northern blot analysis showed that *CGT* mRNA was absent from the homozygous animals, expression of mRNAs for myelin basic protein (MBP), proteolipid protein (PLP), and myelin-associated glycoprotein (MAG) was not significantly diminished in the −/− animals compared with the +/− and +/+ animals (Figure 1C). Consistent with the Northern blot analysis, immunocytochemical analysis of PND 24 cerebellum and spinal cord tissue sections showed extensive expression of MBP (data not shown). Electron microscopy of the optic nerve of PND 24 animals showed that myelin was indeed formed in −/− animals (Figure 3B). Myelin in −/− animals exhibited the characteristic ultrastructure of compact myelin, including the major dense line and intraperiod line (Figure 3D). Similar results were seen with dorsal and ventral columns of spinal white matter (data not shown), and no difference was observed between +/+ and −/− PND 43 sciatic nerve (Figure 3F).

To quantitate the extent of myelination in the PND 24 mutant animals, morphometric analysis was performed on nerve fibers from optic nerve, sciatic nerve, and the dorsal and ventral columns of the spinal white matter (Table 1). The majority of axons in all fields of −/− animals analyzed were myelinated. No difference was notable between mutant and control animals in the extent of myelination in fibers derived from the optic and sciatic nerves. A subtle reduction in myelin thickness was notable in the dorsal column of spinal white matter. In the ventral white matter, the mean myelin thickness was reduced by ~30%, and the ratio of axon diameter to fiber diameter (g) slightly increased in −/− animals compared with +/+ animals.

HFA-GlcC Is Present in Myelin

Consistent with the histological and ultrastructural evidence, myelin was isolated at nearly 50% of the normal yield from two pooled PND 24 and 26 −/− brains (+/+, 9.5 mg/g; −/−, 4.5 mg/g). The altered myelin lipid composition likely contributed to the reduced myelin yield from the mutant animals. Ultrastructural analysis of both +/+ and −/− preparations showed myelin lamellae with major dense lines and intraperiod lines (data not shown). Furthermore, TLC analysis of the lipids present in the myelin preparation showed a pattern very similar to that of the whole brain tissue (Figure 4). As expected, no GalC or sulfatide could be detected in the −/− myelin. HFA-GlcC was present in myelin at a similar proportion as NFA-GalC in the wild-type myelin. Finally, the myelin fraction isolated from −/− brains contained a much greater amount of HFA-sphingomyelin than normal NFA-sphingomyelin (Figure 4).

Nerve Conduction Is Disrupted in *Cgt*$^{-/-}$ Mice

Since the clinical phenotype was suggestive of a disruption of nerve conduction, we measured action potential conduction in the spinal cord of PND 24–28 mice and found that amplitude of the compound action potential in −/− spinal cord was smaller and exhibited a longer latency than that in +/+ control (Figure 5B; Table 2). In addition, the compound action potential in −/− spinal cord was composed of distinct subcomponents, and

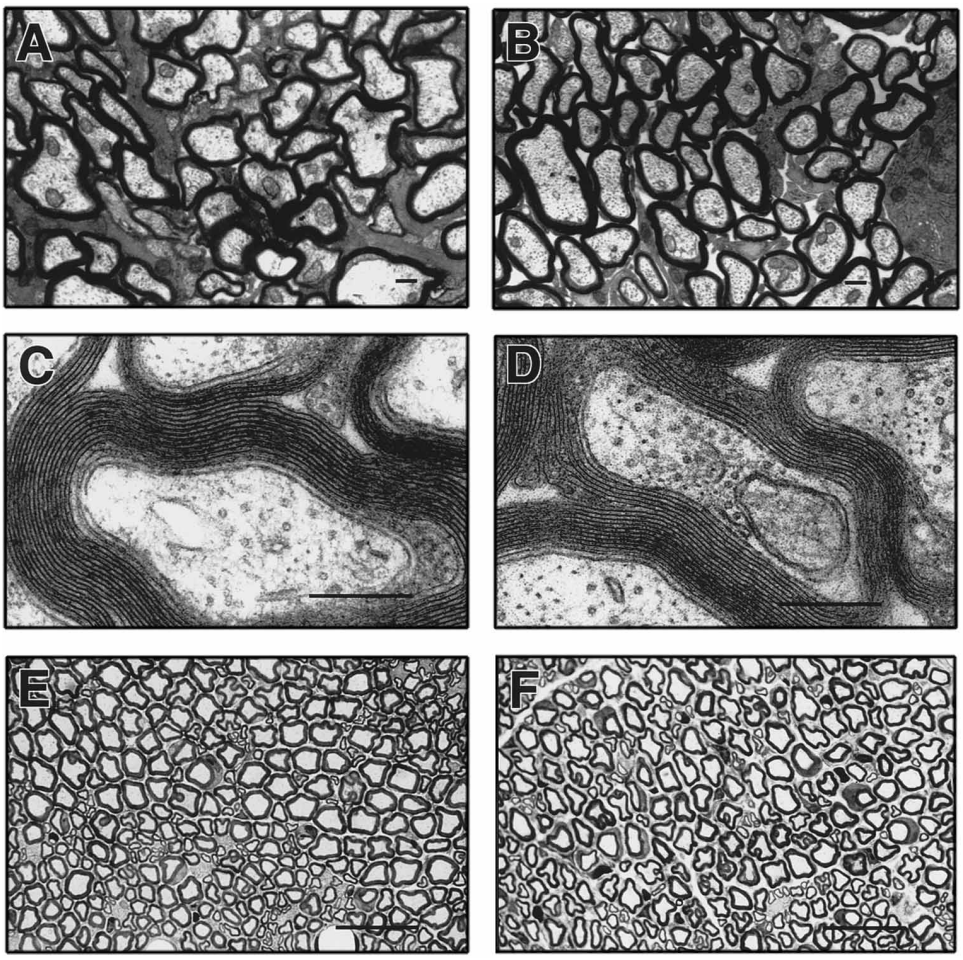

Figure 3. Ultrastructural Analysis of Myelination in Optic and Sciatic Nerves

(A–D) Electron microscopy of PND 24 optic nerve are shown. (A) and (C), +/+; (B) and (D), −/− . Bars: (A) and (B), 0.5 μm; (C) and (D), 0.25 μm. (E and F) Toluidine blue–stained sections (1 μm) from the PND43 sciatic nerve are shown. (E), +/+; (F), −/−. Bar, 25 μm.

Table 1. Morphometric Analysis of Myelination in PND 24 −/− Mice

Nerve fibers	Parameter	+/+	−/−	*p*
Optic	Axon diameter	1.19 ± 0.37	1.17 ± 0.39	NS
	Fiber diameter	1.42 ± 0.39	1.39 ± 0.42	NS
	Myelin thickness	0.11 ± 0.02	0.11 ± 0.02	NS
	g	0.84 ± 0.04	0.84 ± 0.03	NS
Dorsal white matter	Axon diameter	1.26 ± 0.38	1.28 ± 0.40	NS
	Fiber diameter	1.52 ± 0.46	1.51 ± 0.44	NS
	Myelin thickness	0.13 ± 0.05	0.12 ± 0.04	<0.05
	g	0.81 ± 0.03	0.84 ± 0.05	<0.005
Ventral white matter	Axon diameter	1.98 ± 1.39	2.01 ± 1.50	NS
	Fiber diameter	2.36 ± 1.39	2.26 ± 1.57	NS
	Myelin thickness	0.19 ± 0.10	0.13 ± 0.05	<0.00001
	g	0.82 ± 0.05	0.86 ± 0.05	<0.00001
Sciatic	Axon diameter	4.01 ± 1.18	4.02 ± 1.03	NS
	Fiber diameter	5.43 ± 1.56	5.49 ± 1.28	NS
	Myelin thickness	0.71 ± 0.22	0.73 ± 0.17	NS
	g	0.74 ± 0.04	0.73 ± 0.04	NS

A total of 150 fibers from the indicated nerves of two animals for each genotype was analyzed morphometrically. Mean values are shown for the indicated parameters. Units for diameter and thickness measurements are in micrometers. The g value corresponds to the ratio of axonal diameter to fiber diameter and reflects the extent to which myelin thickness is affected by axon diameter. This value has been found to vary between 0.6 and 0.8 depending on the type of nerve fiber and age of the animal (Little and Heath, 1994). Statistical analysis consisted of single factor ANOVA. NS indicates that the data from the control and mutant animals were not significantly different.

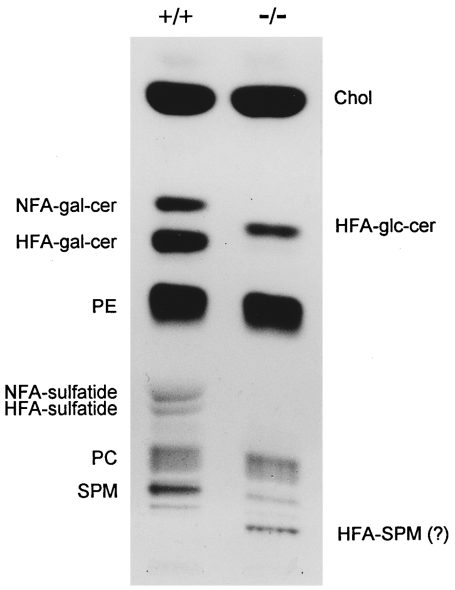

Figure 4. Analysis of Myelin Lipids

Myelin was purified from brain of *Cgt* +/+ and −/− mice. Total lipid fractions from isolated myelin were applied to an untreated HPTLC 60 plate at 285 μg dry myelin equivalent (estimated 200 μg total lipid at 70%) and chromatographed in chloroform-methanol-water (70:30:4). Bands were visualized by copper acetate spray and heating. Abbreviations: NFA, normal fatty acid; HFA, α-hydroxy-fatty acid; glc-cer, glucocerebroside; Chol, cholesterol; PE, ethanolamine phospholipids; PC, choline phospholipids; SPM, sphingomyelin.

the depolarizing afterpotential was reduced in amplitude and duration when compared to +/+ control (Figure 5B; Table 2). Furthermore, the reduction in amplitude of the compound action potential associated with increase in measurement temperature to 37°C from 25°C was proportionally greater in −/− spinal cord (Table 2). Finally, superfusion with 100 μM 4-aminopyridine (4-AP), a blocker of fast K^+ channels, had no effect on the amplitude of the compound action potential of +/+ spinal cord and registered a small increase of depolarizing afterpotential amplitude (Figure 5C). In contrast, superfusion of the −/− spinal cord with 100 μM 4-AP resulted in a reversible increase in amplitude and duration of the compound action potential (Figure 5D).

Myelin in *Cgt*$^{-/-}$ Mice Shows Regional Instability

At PND 24, little pathology was notable in −/− animals except for a small amount of vacuolation in the ventral columns of the spinal cord (Figure 6B). Electron micrographs revealed that ~10% of the axonal processes in this region exhibited mild myelin splitting, compared with ~2% in control animals (data not shown). Splitting was restricted to the sheaths of the large caliber axons. In contrast, PND 43 −/− animals exhibited extensive vacuolation in the ventral columns of the spinal white matter (Figure 6D). At PND 43 splitting was observed in the myelin sheath of virtually every large caliber process, and the extent of splitting was dramatically more severe than at PND 24 (Figures 6E and 6F). Some vacuolation

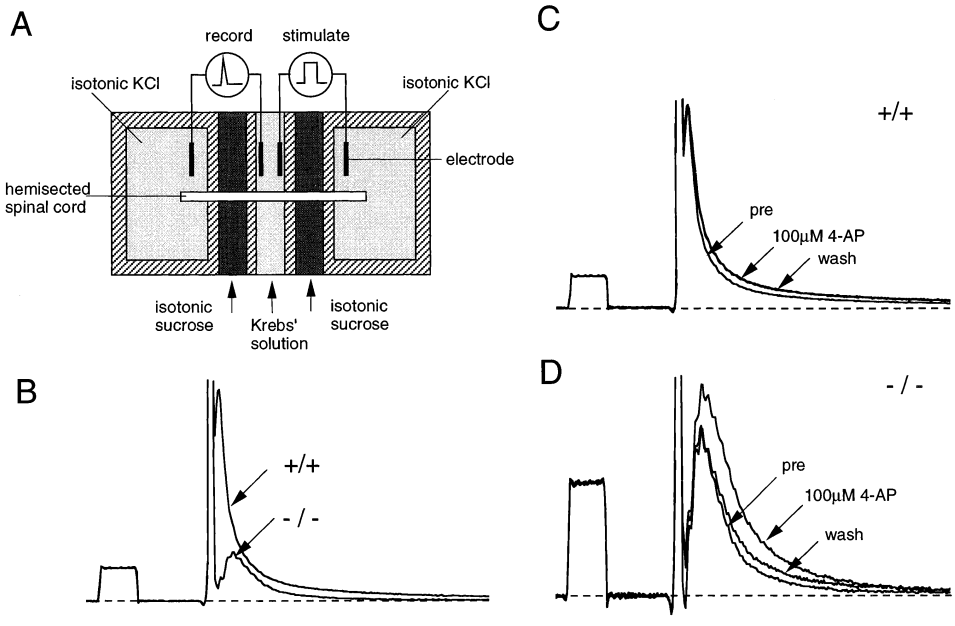

Figure 5. Action Potential Conduction in *Cgt*$^{-/-}$ Mice

(A) Diagram of the recording apparatus. The hemisected spinal cord was placed in a Plexiglas chamber, with the central channel (3.5 mm wide) superfused by flowing, oxygenated Krebs' solution and the two ends isolated by sucrose gaps in chambers containing isotonic (120 mM) potassium chloride solution. Silver/silver chloride electrodes were used to record the potential across one gap and to stimulate the spinal cord across the other.

(B) The compound action potential recorded in the *Cgt* −/− and +/+ spinal cord are shown.

(C and D) The effect of superfusion with 100 μM 4-aminopyridine (4-AP) on the compound potential in +/+ (C) and −/− (D) spinal cord is shown.

The calibration pulse preceding the stimuli in all traces was 1 mV and 1 ms.

Table 2. Characteristics of Compound Action Potentials in *Cgt*$^{-/-}$ Spinal Cord

	+/+	−/−
Amplitude at 37°C (mV)	9.5 ± 1.5	2.5 ± 0.6
Amplitude Reduction (%) after Temperature Increase from 25°C to 37°C	37.4 ± 3.9	61.8 ± 5.8
Peak latency (ms)	0.18 ± 0.03	0.55 ± 0.04
Response to 4-AP (% amplitude increase)	4.0 ± 1.1	25 ± 4.7
Absolute refractory period (ms)	0.45 ± 0.04	1.07 ± 0.10

Compound action potentials were recorded from spinal cords isolated from +/+ and −/− animals (n = 4 per group). Mean values with (SEM) are reported. Variables were significantly different between wild type and mutant ($p < 0.05$, ANOVA).

was observed in the PND 43 optic nerve, but not to the same extent as in the spinal cord (data not shown). Electron microscopy of the −/− spinal cord showed myelin lamellae splitting along the intraperiod line (Figures 6E and 6F) and occasionally by dilated periaxonal space (data not shown). No pathology was observed in the dorsal white matter (data not shown) or sciatic nerves of PND 43 −/− animals (Figure 3F).

Discussion

We have initiated studies directed at determining the function of GalC and sulfatide in myelin formation and maintenance. To this end, we used gene targeting to generate mice deficient in CGT, the enzyme responsible for GalC biosynthesis (Morell and Radin, 1969). Mice lacking CGT cannot synthesize GalC or sulfatide (Figure 2) but are able to form compact myelin (Figure 3). That

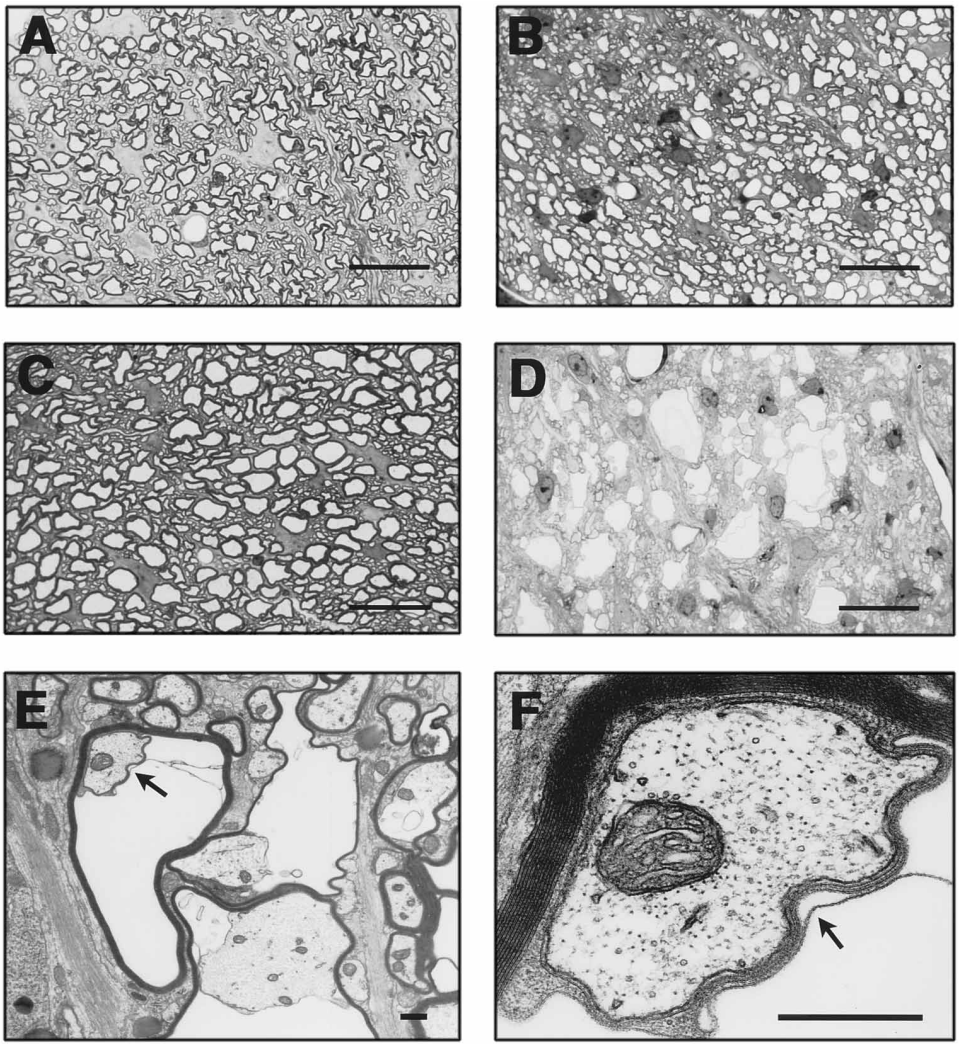

Figure 6. Ultrastructural Analysis of Spinal Cord in PND 24 and 43 *Cgt*$^{-/-}$ Mice

(A–D) Toluidine blue–stained sections (1 μm) from the ventral column of the spinal cord from PND 24 (A and B) and PND 43 (C and D) animals are shown. (A) and (C), +/+; (B) and (D), −/− . Bar, 25 μm.

(E and F) Electron microscopy of selected regions of the ventral column of the spinal cord from PND 43 −/− animals are shown. The arrows indicate regions of myelin splitting. Bar, 0.5 μm.

CGT-deficient mice are able to form myelin was surprising. Given Bansal and Pfeiffer's (1989) observation that oligodendrocyte differentiation was reversibly inhibited by antibodies to GalC, we anticipated that oligodendrocyte development would be disrupted in these mice. Clearly, our findings show that oligodendrocyte differentiation is not grossly affected by the absence of GalC or sulfatide. Other studies have also suggested that GalC may function as a signaling molecule by opening calcium channels in cultured oligodendrocytes (Dyer and Benjamins, 1988, 1989, 1990, 1991). While these in vitro studies convincingly demonstrated that anti-GalC antibodies can trigger influx of calcium and subsequent cytoskeletal rearrangement, our data cast doubt on the in vivo relevancy of these findings. If GalC is a signaling molecule, it cannot be vital to oligodendrocyte development and differentiation, and as a consequence, to myelination.

One explanation for the ability of CGT-deficient mice to form myelin stems from our finding that glucocerebroside (GlcC) is present in myelin of these animals (Figure 4), although only at ~20% of the normal total galactolipids. The relative abundance of HFA-GlcC is unusual given that the amount of GlcC in the normal mouse brain is minuscule, owing to its utilization in ganglioside biosynthesis (Hammarström, 1971). The α-hydroxy ceramide normally destined for HFA-GalC is most likely used for the synthesis of HFA-GlcC and HFA-sphingomyelin in the CGT-deficient animals. Biochemically, GlcC exhibits properties similar to GalC. In vitro, GalC and GlcC form highly stable lamellar phases that require high temperature (80°C–90°C) to disrupt (Koynova and Caffrey, 1995). This thermodynamic similarity would suggest that GlcC may be able to substitute for the structural function attributed to GalC (Curalto, 1987). In contrast, biochemical properties of HFA-sphingomyelin are unclear since this is the first report of this lipid.

Despite the presence of compact myelin in the mutant animals, the electrophysiological analysis showed that nerve function in the spinal cord is disrupted (Figure 5; Table 2). The characteristics of compound action potentials recorded from −/− mice are consistent with a defect in the insulative capacity of myelin. One contributing factor to such a defect would be reduction in the radial impedance (decrease in resistance and/or increase in capacitance) of the myelin sheath. Such a reduction would increase leakage of action current along the internode, reduce the safety factor for conduction, and decrease conduction velocity (Blight, 1985). In addition, impedance alteration would likely lead to a conduction block in a proportion of nerve fibers, further reducing the amplitude of the compound action potential. This effect would be amplified at higher temperatures because of the faster kinetics of ion channels (Frankenhaeuser and Moore, 1963), as is seen in the −/− spinal cord (Table 2).

An additional effect of increased depolarization in the internodal axolemma during the action potential would be the activation of the fast voltage-dependent K^+ channels located in this membrane (Black et al., 1990; Waxman and Ritchie, 1993). These channels are occluded by the myelin sheath and ordinarily do not participate in the conduction process. Their activation would reduce the amplitude and duration of the depolarizing afterpotential, since this potential appears to be based normally on the slow passive discharge of the internodal axolemma (Barrett and Barrett, 1982; Blight, 1985; David et al., 1995). The sensitivity of the −/− action potential to the K^+ channel blocker 4-AP reflects this increased activation and also indicates that there are alterations in the myelin sheath that allow exposure of the channels to the drug.

While it is clear that the electrophysiological properties of the myelin sheath are altered and that the mutant animals are clinically severely affected, these changes might be attributable to structurally abnormal myelin, to hypomyelination, or to compositional changes of the sheath. Nevertheless, the microscopic and morphometric analyses clearly show well-formed and relatively normal amounts of myelin in the −/− mice. While the thickness of myelin in the ventral white matter of −/− animals is reduced to 70% of controls, it seems unlikely that such minor regional hypomyelination could be responsible for the profound clinical and electrophysiological effects observed. Indeed, studies of the shiverer mouse—which is characterized by extensive hypomyelination resulting from disruption of MBP expression—have shown that the defect can be corrected with myelin levels at <50% of normal (Readhead et al., 1987). Moreover, the detailed morphometric analysis of optic nerves of animals that express graded levels of myelin demonstrate that myelin thickness at <50% of control are sufficient for a normal phenotype (Shine et al., 1992). Given these quantitative observations, it seems unlikely that the slight and regional hypomyelination observed in the *Cgt*$^{-/-}$ animals can account for the severe clinical and electrophysiological defects. Rather, it seems more likely that the compositional change in myelin lipids in the −/− animals is responsible for the physiological defects. While the substitution of GlcC may allow for myelination to occur, the absence of GalC likely has profound effects on the physiological properties of the sheath. Furthermore, the absence of sulfatide may also have detrimental consequences on the insulative properties of myelin.

In addition to the compositional changes in myelin, myelin splitting likely contributes to the clinical phenotype of the older *CGT*$^{-/-}$ animals. This pathology exhibited a notable progression with very little myelin splitting in the spinal cord at PND 24 (Figure 5B) and extensive splitting in the ventral columns of the spinal cord of PND 43 animals (Figure 5D). Indeed the localization of the splitting to the ventral columns is striking and may account for the profound hindlimb paralysis typical of older animals, since many of the large caliber axons in the ventral white matter are likely motor neurons. Furthermore the striking localization of this pathology to the ventral white matter raises interesting issues regarding the nature of myelin within different regions of the CNS.

Similar myelin instability has been observed in aspartoacylase deficiency (Canavan disease) in humans (Adachi et al., 1972; Beaudet, 1995) and varieties of toxic demyelination resulting from exposure to triethyltin, hexachlorophene, and cuprizone (Aleu et al., 1963; Suzuki and Kikkawa, 1969; Towfighi et al., 1974; Towfighi, 1980; Watanabe, 1980). In these instances, myelin splits along the intraperiod line possibly as a result of interstitial edema (Aleu et al., 1963; Adachi et al., 1972; Towfighi

et al., 1974; Towfighi, 1980; Watanabe, 1980). While our data do not rule out interstitial edema as a cause of splitting, the absence of GalC and sulfatide from the external leaflet of the plasma membrane must also be a contributing factor. While GlcC is present, it may be insufficiently adhesive or may not be sufficiently abundant to maintain the integrity of the sheath. Furthermore, the absence of the highly charged sulfate moieties contributed by sulfatide may further compromise the adhesive properties of the external leaf of the myelin membrane. Nevertheless, the absence of pathology in the dorsal region of the spinal cord and in the sciatic nerve suggests a heterogeneity in the tolerance of galactolipid elimination from myelinating glia in these animals. Future studies will be directed at clarifying the mechanism of myelin splitting in −/− mice.

In addition to providing clues to the function of GalC and sulfatide in myelin formation and maintenance, these studies have resolved two lingering questions regarding the biosynthesis of GalC and sulfatide. First, our findings clearly show that only one enzyme exists that catalyzes the synthesis of both NFA- and HFA-GalC (Figure 3). Our findings are consistent with and further extend a recent study demonstrating that CGT is capable of catalyzing the synthesis of both NFA- and HFA-GalC in vitro (Schaeren-Wiemers et al., 1995). This study eliminated the need to postulate a second enzyme to account for the known acceptor specificity, but did not exclude the possibility for a second enzyme. Our results clearly exclude the existence of another enzyme. Second, our findings confirmed the generally accepted notion that GalC is the exclusive precursor for synthesis of sulfatide.

While abundantly expressed in myelinating glia, GalC and sulfatide have also been identified in other cell types. In neuronal tissue, these lipids are present in axolemma (De Vries et al., 1972), and CGT expression has been identified in a subset of motor neurons (Schaeren-Wiemers et al., 1995). Other studies have shown that GalC is expressed in peripheral tissues including kidney (Costantino-Ceccarini and Morell, 1973) and colonic epithelia, where it may serve as an alternate receptor for HIV in the absence of CD4 expression (Harouse et al., 1991; Yahi et al., 1992; Long et al., 1994). Furthermore, sulfatide is expressed in islets of Langerhans and kidney glomeruli—tissues that are affected by diabetic disease, possibly as suggested by Buschard et al. (1994) as a result of anti-sulfatide antibodies. While the functions of GalC and sulfatide in these settings remain unclear, the availability of CGT-deficient mice should provide a means to better explore this issue.

Together, the data presented provide the first glimpses into the function of GalC and sulfatide in myelin formation, function, and maintenance. Indeed, the results of our studies show that the CGT-deficient mice are distinctive from the naturally occurring and experimentally induced myelin mutants that are typified by extensive hypomyelination or dysmyelination (Campagnoni and Macklin, 1988; Giese et al., 1992; Boison and Stoffel, 1994; Li et al., 1994; Montag et al., 1994; Adlkofer et al., 1995; Lunn et al., 1995). Our results clearly demonstrate ultrastructurally normal myelin can be formed in the absence of GalC and sulfatide. Nevertheless, the dramatically altered electrophysiological properties observed in these mice indicate an intrinsic role for these lipids in the insulative properties of myelin. Furthermore, the observed myelin instability clearly implicates GalC and sulfatide in stabilizing the ultrastructure of the myelin sheath. The availability of the CGT-deficient animals should allow for the further analysis of these and other important functions of GalC and sulfatide.

Experimental Procedures

Construction of *Cgt* Targeting Vector

The genomic organization of the mouse *Cgt* gene has been described (Coetzee et al., 1996). Exon 2 was chosen as a target for disruption since it codes for the N-terminal half of the CGT enzyme, and because a KpnI site resides 219 nt downstream of the ATG which would facilitate construction of the targeting vector. A 14.5 kb λ genomic clone carrying exon 2 and flanking intronic sequences was subcloned into the SalI site of plasmid pBSSK(+) (pCGTE2) (Stratagene). Subsequently, a 3.5 kb KpnI fragment (E2KK3.5), containing 3.3 kb of intron I and the first 0.2 kb of exon 2, and a 7.0 kb KpnI/SalI fragment (E2KS7) harboring the remainder of exon 2 and intron 2 were subcloned from pCGTE2 into plasmid pBSSK(+). The parental plasmid for the targeting construct was plasmid pPNT, which carries pGK-neo-poly(A), herpes simplex virus thymidine kinase, and multiple cloning sites flanking the neo cassette (Tybulewicz et al., 1991). The targeting vector, pPNTCGT, was generated in a two-step cloning process. First, fragment E2KS7 was digested with KpnI, blunt-ended with T4 DNA polymerase, followed by NotI digestion. This fragment was subcloned into the NotI and blunted XhoI sites upstream of the neo cassette. Subsequently, fragment E2KK3.5 was subcloned into the KpnI site downstream of the neo cassette. Orientation was determined by PCR and diagnostic restriction digestion.

Generation of *Cgt*$^{-/-}$ Mice

NotI-digested pPNTCGT was electroporated into BK4 ES cells, a subclone of E14TG2a cells. Neo-resistant clones were isolated using G418 and standard ES culture methods. Fifty-two neo resistant clones were screened for the correct recombination event by Southern blot hybridization using probe A (Figure 1A). Fourteen positive clones were identified and one (#33) injected into C57Bl/6J blastocysts. Male chimeric mice were bred with C57Bl/6 females, and agouti offspring screened for transmission of the disrupted allele by Southern blot hybridization using probe B (Figure 1A). Homozygotes were generated by interbreeding of heterozygote F1 mice. For Southern blot analysis, 5–10 μg of tail or ES DNA was digested with BamHI, separated by agarose gel electrophoresis, transferred to Zeta-Probe (Bio-Rad) using 0.4 N NaOH. Probes were labeled by PCR (Jansen and Ledley, 1989), and hybridization and washes performed as previously described (Coetzee et al., 1996).

RNA Analysis

Total RNA was prepared from PND 24 brains using the guanidinium thiocyanate method of Chirgwin et al. (1979). Northern blots were prepared as described by Popko et al. (1987). Probes for CGT (Coetzee et al., 1996), neo (Tybulewicz et al., 1991), MAG (Sutcliffe et al., 1983), MBP (Roach et al., 1983), and PLP (Milner et al., 1985), were prepared by PCR as described above. Hybridization and washes were performed as previously described (Popko et al., 1987). A pair of oligonucleotides for 18S ribosomal RNA were end-labeled with digoxigenin and used to evaluate relative levels of total RNA present in each lane. Preparation of the oligonucleotide probe, hybridization, and wash conditions followed the instructions of the manufacturer (Boehringer-Mannheim).

Lipid Analysis

Tissues were weighed and extracted with 20 volumes of chloroform-methanol (2:1, v/v) (Folch-Pi et al., 1957). Insoluble materials were removed by centrifugation. The extract was partitioned with addition of 0.2 volume of water, the upper phase discarded and the lower

phase washed once with the pure solvent upper phase (chloroform-methanol-water, 4:48:47, v/v/v) and dried under a stream of nitrogen. The dried lipid was dissolved in chloroform-methanol (2:1, v/v) at 1 ml/100 mg tissue. The total lipid fractions were first chromatographed on thin-layer plate (HPTLC 60, Merck) at 20 μl (2 mg wet weight tissue) per sample in the solvent system of chloroform-methanol-water (70:30:4) and lipid bands visualized with copper acetate spray and heating (3% copper acetate in 15% phosphoric acid). Then the lipids were subjected to the mercuric chloride-saponification procedure (Abramson et al., 1965) in order to degrade essentially all glycerophospholipids. After solvent partitioning, the lower lipid phase contained sphingolipids, cholesterol, and the liberated free fatty acids. This fraction was dissolved in chloroform-methanol (2:1, v/v/) at 1 ml/100 mg wet tissue and then examined by the same thin-layer chromatographic system above, and also by borate-impregnated thin-layer chromatography in the solvent system of chloroform-methanol-concentrated ammonia (70:30:5, v/v/v) at 30 μl (3 mg wet tissue) per sample. Borate permeation was done in the vapor phase (Igisu et al., 1983). Lipid bands were visualized either with the copper acetate spray or the anisaldehyde spray (0.5 ml anisaldehyde, 49 ml acetic acid, and 1 ml concentrated sulfuric acid) and heating. The latter spray gave differential colors for cholesterol, glycolipids, glycerophospholipids, and sphingomyelin.

Myelin was isolated by centrifugation over a discontinuous sucrose gradient following standard procedures (Norton and Poduslo, 1973). A sample of each isolated myelin fraction was processed for electron microscopic examination of myelin structure. The remainder of the fractions were lyophilized. Lyophilized myelin fractions were extracted with 4 ml of chloroform-methanol (2:1, v/v) after being suspended in 0.2 ml of water. The lipids were examined by the same thin-layer chromatography system as above at 200 μg total lipid per sample, estimated by an assumption that 70% of dry myelin is lipid.

Histological Analysis

For toluidine blue staining of 1 μm sections and electron microscopy, optic nerve, cervical spinal cord, and sciatic nerve were removed from mice perfused through the left cardiac ventricle with an ice-cold solution of 4% paraformaldehyde and 2.5% gluteraldehyde in 0.1 M sodium phosphate buffer (pH 7.4). Tissues were immersion fixed overnight at 4°C in the same fixative solution. Tissues were processed, embedded, sectioned, and analyzed by light, electron microscopy, and immunocytochemistry as previously described (Fujita et al., 1996).

Morphometric analysis of myelination was performed on nerve fibers selected from random fields of electron micrographs of optic nerve (specimen taken 1.75 mm anterior to optic chiasmata), dorsal, and ventral cervical spinal white matter taken at the magnification of 5000 or 10,000. Sciatic nerve fibers were selected from random fields of toluidine blue sections. Two +/+ and −/− animals were used for these analyses. Micrographs were scanned and morphometry performed on a Macintosh Quadra 840AV computer using the NIH IMAGE v1.54 software package as previously described (Rath et al., 1995).

For analysis of myelin periodicity, electron micrographs of selected myelinated fibers from optic nerve and ventral spinal cord were taken at the magnification of 40,700 and analyzed using NIH IMAGE v1.54 software package.

Electrophysiology

Conduction properties of myelinated axons were examined in acutely isolated, hemisected spinal cords of *Cgt* −/− and +/+ mice, using a double sucrose-gap technique. This provided a stable recording and stimulating arrangement with a fixed conduction distance of 3.5 mm in the thoracic spinal cord. The animals were anesthetized with an intraperitoneal injection of ketamine HCl 60 mg/kg, xylazine 10 mg/kg, and acepromazine maleate 0.6 mg/kg. They were then decapitated and the spinal cord extracted by rapid laminectomy and washed in oxygenated Krebs' solution (NaCl 124 mM, KCl 2 mM, KH_2PO_4 1.2 mM, $MgSO_4$ 1.3 mM, $CaCl_2$ 1.2 mM, dextrose 10 mM, $NaHCO_3$ 26 mM, sodium ascorbate 6 mM, equilibrated with 95% O_2, 5% CO_2). The cord was divided along the sagittal midline with a scalpel blade and the two halves incubated in oxygenated Krebs' solution at room temperature for at least 1 hr, then mounted in a recording chamber, as illustrated in Figure 7A. The temperature of the chamber was raised to 37°C, and a series of recordings made of the response to stimulation over a range of intensities and interpulse intervals. The data were digitized and recorded on videotape for subsequent analysis using customized Labview software on a Power Macintosh computer. 4-aminopyridine (Regis Technologies, Morton Grove, IL) was dissolved in the Krebs' solution, at pH 7.3.

Acknowledgments

Correspondence should be addressed to Brian Popko. We thank Clarita Langaman and Teresa Bone-Turrentine for assistance with electron microscopy and histological analysis, April Kemper for myelin preparation, Tom Kelly for assistance with electrophysiology, and Dr. Robert Bagnell for assistance with morphometry. We also thank Dr. Beverly Koller and the UNC embryonic stem cell facility for generating the chimeric mice. This work was supported by a grant, R62595, from the National Multiple Sclerosis Society (B. P.); grants NS27336 (B. P.), NS24453 (K. S.), NS24289 (K. S.), and NS33687 (A. B.) from the National Institutes of Health (NIH); and a Mental Retardation Research Center core grant (HD03110) from the NIH. B. P. is the recipient of a Research Career Development Award from the NIH (NS01637). J. D. is supported by a training grant, HD07201, from the NIH. T. C. is a recipient of an Advanced Postdoctoral Fellowship from the National Multiple Sclerosis Society. N. F. was supported by a grant from the International Human Frontiers Science Organization. R. S. was supported by a fellowship from the Canadian Spinal Research Organization.

Received April 15, 1996; revised June 4, 1996.

References

Abramson, M.B., Norton, W.T., and Katzman, R. (1965). Study of ionic structure in phospholipids by infrared spectra. J. Biol. Chem. *240*, 2389–2395.

Adachi, M., Torii, J., Schneck, L., and Volk, B.W. (1972). Electron microscopic and enzyme histochemical studies of the cerebellum in spongy degeneration (Van Bogaert and Bertrand type). Acta. Neuropathol. *20*, 22–31.

Adlkofer, K., Martinin, R., Aguzzi, A., Zielasek, J., Toyka, K.V., and Suter, U. (1995). Hypermyelination and demylinating peripheral neuropathy in *Pmp*-22-deficient mice. Nature Genet. *11*, 274–280.

Aleu, F.R., Katzman, R., and Terry, R.D. (1963). Fine structure and electrolyte analysis of cerebral edema induced by alkyltin intoxication. J. Neuropathol. Exp. Neurol. *22*, 403–413.

Bansal, R., and Pfeiffer, S. (1989). Reversible inhibition of oligodendrocyte progenitor differentiation by a monoclonal antibody against surface galactolipids. Proc. Natl. Acad. Sci. USA *86*, 6181–6185.

Barrett, E.F., and Barrett, J.N. (1982). Intracellular recording from vertebrate myelinated axons: mechanism of the depolarizing afterpotential. J. Physiol. *323*, 117–144.

Beaudet, A.L. (1995). Aspartoacylase deficiency (Canavan Disease). In The Metabolic and Molecular Basis of Inherited Disease, 7th Edition. C.R. Scriber, A.L. Beaudet, W.S. Sly, and D. Valle, eds. (New York: McGraw Hill, Inc.), pp. 4599–4605.

Benjamins, J.A., and Dyer, C.A. (1990). Glycolipids and transmembrane signaling in oligodendroglia. Ann. NY Acad. Sci. *605*, 90–100.

Black, J.A., Kocsis, J.D., and Waxman, S.G. (1990). Ion channel organization of the myelinated fiber. Trends Neurosci. *13*, 48–54.

Blight, A.R. (1985). Computer simulation of action potentials and afterpotentials in mammalian myelinated axons: the case for a lower resistance myelin sheath. Neuroscience *15*, 13–31.

Boison, E., and Stoffel, W. (1994). Disruption of the compacted myelin sheath of axons of the central nervous system in proteolipid protein-deficient mice. Proc. Natl. Acad. Sci. USA *91*, 11709–11713.

Buschard, K., Josefsen, K., Hansen, S.V., Thorn, T., Marshall, M.O., Persson, H., Mansson, J.-E., and Fredman, P. (1994). Sulphatide in

islets of Langerhans and in organs affected in diabetic late complications: a study in human and animal tissue. Diabetologia *37*, 1000–1006.

Campagnoni, A.T., and Macklin, W.B. (1988). Cellular and molecular aspects of myelin protein gene expression. Mol. Neurobiol. *2*, 41–89.

Chirgwin, J.M., Przybyla, A.E., MacDonald, R.J., and Rutter, W.J. (1979). Isolation of biologically active ribonucleic acid from sources enriched in ribonuclease. Biochemistry *18*, 5294–5299.

Coetzee, T., Li, X., Fujita, N., Marcus, J., Suzuki, K., Francke, U., and Popko, B. (1996). Molecular cloning, chromosomal mapping, and characterization of the mouse UDP-galactose:ceramide galactosyltransferase gene. Genomics, in press.

Costantino-Ceccarini, E., and Morell, P. (1973). Synthesis of galactosylceramide and glucosylceramide by mouse kidney preparations. J. Biol. Chem. *248*, 8240–8246.

Curalto, W. (1987). Glycolipid function. Biochim. Biophys. Acta *906*, 137–160.

David, G., Modney, B., Scappaticci, K.A., Barrett, J.N., and Barrett, E.F. (1995). Electrical and morphological factors influencing the depolarizing after-potential in rat and lizard myelinated axons. J. Physiol. *489*, 141–157.

De Vries, G.H., Norton, W.T., and Raine, C.S. (1972). Axons: isolation from mammalian central nervous system. Science *175*, 1370–1372.

Dorfman, S., Fry, J., and Silberberg, D. (1979). Antiserum induced myelination inhibition in vitro without complement. Brain Res. *177*, 105–114.

Dyer, C.A. (1993). Novel oligodendrocyte transmembrane signaling systems. Mol. Neurobiol. *7*, 1–22.

Dyer, C.A., and Benjamins, J.A. (1988). Antibody to galactocerebroside alters organization of oligodendroglial membrane sheets in culture. J. Neurosci. *9*, 4307–4310.

Dyer, C.A., and Benjamins, J.A. (1989). Organization of oligodendroglial membrane sheets. II: galactocerebroside:antibody interactions signal changes in cytoskeleton and myelin basic protein. J. Neurosci. Res. *24*, 212–221.

Dyer, C.A., and Benjamins, J.A. (1990). Glycolipids and transmembrane signaling: antibodies to galactocerebroside cause a calcium influx in oligodendrocytes. J. Cell Biol. *111*, 625–633.

Dyer, C.A., and Benjamins, J.A. (1991). Galactocerebroside and sulfatide independently mediate Ca^{2+} responses in oligodendrocytes. J. Neurosci. Res. *30*, 699–711.

Folch-Pi, J., Lees, M.B., and Sloane-Stanley, G.H. (1957). A simple method for the isolation and purification of total lipids from animal tissue. J. Biol. Chem. *226*, 497–509.

Frankenhaeuser, B., and Moore, L.E. (1963). The effect of temperature on the sodium and potassium permeability changes in myelinated nerve fibers of Xenopus laevis. J. Physiol. *169*, 431–437.

Fry, J.M., Weissbarth, S., and Lehrer, G.M. (1974). Cerebroside antibody inhibits sulfatide synthesis and myelination and demyelinates in cord tissue cultures. Science *183*, 540–542.

Fujita, N., Suzuki, K., Vanier, M.T., Popko, B., Maeda, N., Klein, A., Henseler, M., Sandhoff, K., Nakayasu, H., Suzuki, K. (1996). Targeted disruption of the mouse sphingolipid activator protein gene: a complex phenotype, including severe leukodystrophy and wide-spread storage of multiple sphingolipids. Human Molec. Genet. *5*, 711–725.

Giese, K.P., Martini, R., Lemke, G., Soriano, P., and Schachner, M. (1992). Disruption of the P_0 gene in mice leads to hypomyelination, abnormal expression of recognition molecules, and degeneration of myelin and axons. Cell *71*, 565–576.

Hammarström, S. (1971). Brain glucosyl ceramides containing 2-hydroxyacids: identification of molecular species by gas-liquid chromatography-mass spectrometry. Eur. J. Biochem. *21*, 388–392.

Harouse, J.M., Bhat, S., Spitalnik, L., Laughlin, M., Stefeno, K., Silverberg, D.H., and Gonzalez-Scarano, F. (1991). Inhibition of entry of HIV-1 in neural cell lines by antibodies against galactosyl ceramide. Science *253*, 320–323.

Igisu, H., Takahashi, H., Suzuki, K., and Suzuki, K. (1983). Abnormal accumulation of galactosylceramide in the kidney of twitcher mouse. Biochem. Biophys. Res. Commun. *110*, 940–944.

Jansen, R., and Ledley, F.D. (1989). Production of discrete high specific activity DNA probes using polymerase chain reaction. Genet. Anal. Tech. Appl. *6*, 79–83.

Koynova, R., and Caffrey, M. (1995). Phases and phase transitions of the sphingolipids. Biochim. Biophys. Acta *1255*, 213–236.

Li, C., Tropak, M.B., Gerlai, R., Clapoff, S., Abramow-Newerly, W., Trapp, B., Peterson, A., and Roder, J. (1994). Myelination in the absence of myelin-associated glycoprotein. Nature *369*, 747–750.

Little, G.J., and Heath, J.W. (1994). Morphometric analysis of axons myelinated during adult life in the mouse superior cervical ganglion. J. Anat. *184*, 387–398.

Long, D., Berson, J.F., Cook, D.G., and Doms, R.W. (1994). Characterization of human immunodeficiency virus type 1 gp120 binding to liposomes containing galactosylceramide. J. Virol. *68*, 5890–5898.

Lunn, K.F., Fanarraga, M.L., and Duncan, I.D. (1995). Myelin mutants: new models and new observations. Micros. Res. Tech. *32*, 183–203.

Milner, R.J., Lai, C., Nave, K., Lenoir, D., Ogata, J., and Sutcliffe, J.G. (1985). Nucleotide sequences of two mRNAs for rat brain myelin proteolipid protein. Cell *42*, 931–939.

Montag, D., Giese, K.P., Bartsch, U., Martini, R., Lang, Y., Blüthmann, H., Karthigasan, J., Kirschner, D.A., Wintergerst, E.S., Nave, K., Zielasek, J., Toyka, K.V., Lipp, H., and Schachner, M. (1994). Mice deficient for the myelin-associated glycoprotein show subtle abnormalities in myelin. Neuron *13*, 229–246.

Morell, P., and Radin, N.S. (1969). Synthesis of cerebroside by brain from uridine diphosphate galactose and ceramide containing hydroxy fatty acid. Biochemistry *8*, 506–512.

Morell, P., Quarles, R.H., and Norton, W.T. (1994). Myelin formation, structure, and biochemistry. In Basic Neurochemistry: Molecular, Cellular, and Medical Aspects. G.J. Siegel, B.W. Agranoff, R.W. Albers, and P.B. Molinoff, eds. (New York: Raven Press), pp. 117–143.

Neskovic, N.M., Roussel, G., and Nussbaum, J.L. (1986). UDP-galactose:ceramide galactosyltransferase of rat brain: a new method of purification and production of specific antibodies. J. Neurochem. *47*, 1412–1418.

Norton, W.T., and Cammer, W. (1984). Isolation and characterization of myelin. In Myelin. P. Morell, ed. (New York: Plenum Press), pp. 147–195.

Norton, W.T., and Poduslo, S.E. (1973). Myelination in rat brain: method of myelin isolation. J. Neurochem. *21*, 749–757.

Pfeiffer, S.E., Warrington, A.E., and Bansal, R. (1993). The oligodendrocyte and its many cellular processes. Trends Cell Biol. *3*, 191–197.

Popko, B., Puckett, C., Lai, E., Shine, H.D., Readhead, C., Takahashi, N., Hunt, S.W.I., Sidman, R.L., and Hood, L. (1987). Myelin deficient mice: expression of myelin basic protein and generation of mice with varying levels of myelin. Cell *48*, 713–721.

Ranscht, B., Wood, P.M., and Bunge, R.P. (1987). Inhibition of in vitro peripheral myelin formation by monoclonal anti-galactocerebroside. J. Neurosci. *7*, 2936–2947.

Rath, E.M., Kelly, D., Bouldin, T.W., Popko, B. (1995). Impaired peripheral nerve regeneration in a mutant strain of mice (*Enr*) with a Schwann cell defect. J. Neurosci. *15*, 7226–7237.

Readhead, C., Popko, B., Takashi, N., Shine, H.D., Saavedra, R.A., Sidman, R.L., Hood, L. (1987). Expression of myelin basic protein in transgenic shiverer mice: correction of the dysmyelinating phenotype. Cell *48*, 703–712.

Roach, A., Boylan, K., Horvath, S., Prusiner, S.B., and Hood, L. (1983). Characterization of cloned cDNA representing rat myelin basic protein: absence of expression in brain of shiverer mutant mice. Cell *42*, 799–806.

Rosenbluth, J., Liu, Z., Guo, D., and Schiff, R. (1994). Inhibition of CNS myelin development in vivo by implantation of anti-GalC hybridoma cells. J. Neurocytol. *23*, 699–707.

Schaeren-Wiemers, N., vander Bijl, P., and Schwab, M.D. (1995). The UDP-galactose:ceramide galactosyltransferase: expression pattern

in oligodendrocytes and Schwann cells during myelination and substrate preference for hydroxyceramide. J. Neurochem. *65*, 2267–2278.

Schulte, S., and Stoffel, W. (1993). Ceramide UDPgalactosyltransferase from myelinating rat brain: purification, cloning and expression. Proc. Natl. Acad. Sci. USA *90*, 10265–10269.

Shine, H.D., Readhead, C., Popko, B., Hood, L., Sidman, R.L. (1992). Morphometric analysis of normal, mutant, and transgenic CNS: correlation of myelin basic protein expression to myelogenesis. J. Neurochem. *58*, 342–349.

Stahl, N., Jurevics, H., Morell, P., Suzuki, K., and Popko, B. (1994). Isolation, characterization, and expression of cDNA clones that encode rat UDP-galactose:ceramide galactosyltransferase. J. Neurosci. Res. *38*, 234–242.

Sutcliffe, J.G., Milner, R.J., Shinnick, T.M., and Bloom, F.E. (1983). Identifying the protein products of brain-specific genes with antibodies to chemically synthesized peptides. Cell *33*, 671–682.

Suzuki, K., and Kikkawa, Y. (1969). Status spongiosus of CNS and hepatic changes induced by cuprizone (biscyclopexanone oxalyldihydrazone). Am. J. Pathol. *54*, 307–325.

Towfighi, J. (1980). Hexachlorophene. In Experimental and Clinical Neurotoxicology. P.S. Spencer and H.H. Schaumburg, eds. (Baltimore: Williams and Wilkins), pp. 440–455.

Towfighi, J., Gonatas, N.K., and McCree, L. (1974). Hexachlorophene-induced changes in central and peripheral myelinated axons of developing and adult rats. Lab Invest. *31*, 712–721.

Tybulewicz, V.L.J., Crawford, C.E., Jackson, P.K., Bronson, R.T., and Mulligan, R.C. (1991). Neonatal lethality and lymphopenia in mice with a homozygous disruption of the c-*abl* proto-oncogene. Cell *65*, 1153–1163.

Watanabe, I. (1980). Organotins. In Experimental and Clinical Neurotoxicology. P.S. Spencer and H.H. Schaumburg, eds. (Baltimore: Williams and Wilkins), pp. 545–557.

Waxman, S.G., and Ritchie, J.M. (1993). Molecular dissection of the myelinated axon. Ann. Neurol. *33*, 121–136.

Yahi, N.S., Baghdiguian, S., Moreau, H., and Fantini, J. (1992). Galactosyl ceramide (or closely related molecule) is the receptor for human immunodeficiency virus type 1 on human colon epithelial HT29 cells. J. Virol. *66*, 4848–4859.